Available online at www.dergipark.org.tr/en

INTERNATIONAL ADVANCED RESEARCHES and ENGINEERING JOURNAL

Journal homepage: www.dergipark.org.tr/en/pub/iarej

e-ISSN: 2618-575X

International Open Access

Volume 04
Issue 02

August, 2020

Research Article

Investigation of plastic zone dimension in front of an external semi-elliptic crack on pipe of molecular bushing

İlyas Kacar [a,*]

[a]*Niğde Ömer Halisdemir University Engineering Faculty, Department of Mechatronics Engineering, Niğde, 51240, Turkey*

ARTICLE INFO

Article history:
Received 10 April 2020
Revised 01 May2020
Accepted 05 May 2020

Keywords:
Fracture mechanics
Molecular bushing
Plastic zone
Semi-elliptical crack
Stress intensity factor
Yield criteria

ABSTRACT

In automotive industry, molecular bushings transfer loads from steering gearbox to wheels on a vehicle. The pipe is one of the most vital member of these routing systems and manufactured using 41Cr4 sheet metal. For a pipe of molecular bushing, analytical solutions of crack tip plastic zone size is derived by using four yield criteria: Von Mises, Tresca, Hill48, and Hu2003. Hill48 and Hu2003 are useful criteria for materials with higher anisotropy such as sheet metals. Material's hardening behaviour is modelled using bilinear isotropic hardening rule by coupling with associated flow rule under isotropic and large scale plasticity condition. The solutions are developed for mode-I loading case due to service conditions of the pipe. A finite element simulation is performed to collect stress intensity factors. Results are verified by comparing to those of Irwin and Dugdale. The plastic zone's shape and size are analysed for different anisotropy cases. The results show that plastic zone have "kidney" or "butterfly" shapes depending on the yield criteria used. Increasing anisotropy has significant effect on plastic zone.

1. Introduction

The suspension system is used to stabilize the vehicle during driving, allowing the wheels to continually follow the road surface to improve steering stability. The molecular bushing is a part of suspension system. It damps the vibration caused by road condition [1]. They are manufactured using 41Cr4 steels in automotive industry. This structural part is subjected to corrosion leading to crack propagation and fracture [2, 3]. Any damage to this part can lead to loss of driving stability and impaired driving comfort.

All of stresses at the crack tip goes to infinity due to singularity because crack tip radius goes to zero. However, the structural materials have a yield strength and therefore the material exhibits plastic deformation when the stress value reaches to its yield strength. So there will be a plastic zone surrounding the crack front. This plastically deformed zone is called the crack front plastic zone. Although it is assumed that the boundary of this zone is just as a simple circle at the beginning of fracture mechanics, actually, it is seen that it has different shapes according to the basis of the yield criterion and the stress distribution (plane strain or plain stress) on the crack tip line.

The plastic zone (PZ) size in the region near the tip of a propagating crack is considered as a measure of the material resistance against crack surfaces opening [4]. The larger plastic zone size results in the higher plastic energy absorption and the higher toughness [5, 6]. Inelastic deformation occurs when the yield strength is exceeded. The crack tip singularity in the linear elastic fracture mechanics (LEFM) cannot be sufficient to give plastic flow based on stress distribution [7, 8]. Because during plastic deformation, the boundary of the plastic region will be different in the proximity of the crack tip. Many studies are being done for the singular terms for the correct estimation of the plastic flow that actually occurs [9].

In this study, a semi-elliptical crack is inserted on the external surface of the pipe of a molecular bushing. PZ equations are derived by using the Von Mises, Tresca, Hill48, and Hu2003 yield criteria using the stress field near crack tip. Subsequently, the stress distribution and stress intensity factors (SIF) are determined in front of the crack

* Corresponding author. Tel.: +90 (388) 225 4648; Fax: +90 (388) 221 0112.
E-mail addresses: ikacar@gmail.com *(İ. Kacar)*
ORCID: 0000-0002-5887-8807 *(İ. Kacar)*
DOI: 10.35860/iarej.717634

by elasto-plastic finite element analysis (FEA). Also crack tip blunting, stress, and strain results from finite element simulation is presented in the paper.

2. Problem Description

A pipe contains a semi-elliptical external surface crack under uniaxial tension. Figure 1 shows the details of a V-arm and the pipe of molecular bushing. So the problem has a mode-I loading case. First elastic stress fields at the crack tip is obtained analytically. Further, PZs are determined by using various anisotropic yield criteria.

The pipe material is 41Cr4 and its chemical composition is given in Table 1.

Anisotropy values and mechanical properties for 41Cr4 are given in Table 2. These parameters are necessary to use in yield criteria. In the table r_θ values are called anisotropy coefficients or Lankford coefficients and determined from tensile test by using samples preparing at 0°, 45°, and 90° directions with respect to main axis.

The material is assumed as linear elastic and perfect plastic where no hardening is seen during plastic deformation. So, the bilinear isotropic hardening (BISO) rule $\sigma(h) = YS + TM(\varepsilon^p)$ is used by taking *YS*=560 MPa and setting TM to zero to ensure perfect plasticity. *YS* is yield strength and *TM* is the tangent modulus, and ε^p is the actual amount of plastic deformation. Both *YS* and *TM* are enough to set the rule. Anisotropic hardening is a potential for further work.

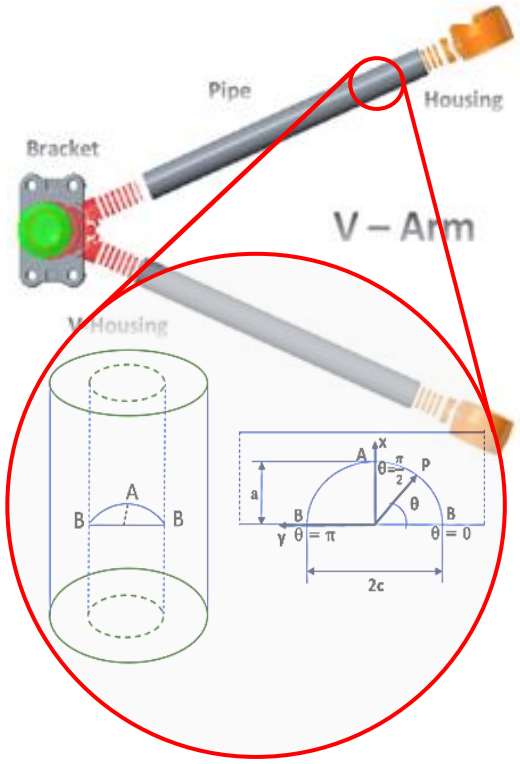

Figure 1. Schematic representation of a semi-elliptical surface crack on the pipe of a molecular bushing

Table 1. Chemical composition of 41Cr4 (EN 1.7035).

C	Si	Mn	Cr	Ni	Al	Cu
0.404	0.349	0.67	0.93	0.061	0.026	0.016

Table 2. Anisotropy values and mechanical properties for 41Cr4 [10, 11].

Material properties		**41Cr4 (EN 1.7035)**
Anisotropy coefficients	r_0	0.9
	r_{45}	1.1
	r_{90}	0.9
Poisson ratio	ν	0.29
Yield strength	σ_y	560 MPa
Elasticity modules	E	215 GPa

3. Analysis

Knowing PZ's size and shape is necessary to analyze the crack initiation angle and its propagation. A crack follows the "easiest" path through the plastic zone based on minimum stress or plastic work depending on criterion used. Due to large scale plastic flow in front of a crack and remaining elastic region of geometry, elasto-plastic fracture mechanics analysis is necessary to determine PZ's border. It will be determined by applying some yield criteria on the stress field in front of a crack.

3.1 Crack Tip Stress Field

The stress singularity is inherently present near the crack tip and SIF depends on this singularity. But a failure criterion in classical solid mechanics is not enough to be able to take care of the stress singularity. Because it is based on stress components and these components are not able to exhibit the stress singularity. But equations (1) can exhibit stress singularity due to the term $\sigma \sim K_I r^{-1/2}$. So the stress can go to infinity by getting closer near the crack tip. Although many stress intensity factor calculation methods have been published in handbooks [12], they are limited to primitive shapes only.

For complex shaped geometries, it is a way to find the stress intensity factor by means of FEA [13, 14]. The singular elastic stress field is shown in Figure 2 where radius *R(θ)* and angle *θ* are the polar coordinate axes at the crack tip for a body including a crack under Mode-I loading [3].

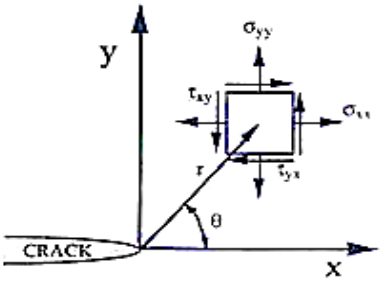

Figure 2. Stress state at crack tip loaded Mode I

$$\sigma_{xx} = \frac{K_I}{\sqrt{2\pi R(\theta)}} cos\left(\frac{\theta}{2}\right)\left[1 - sin\left(\frac{\theta}{2}\right) sin\left(\frac{3\theta}{2}\right)\right]$$
$$\sigma_{yy} = \frac{K_I}{\sqrt{2\pi R(\theta)}} cos\left(\frac{\theta}{2}\right)\left[1 + sin\left(\frac{\theta}{2}\right) sin\left(\frac{3\theta}{2}\right)\right]$$
$$\sigma_{xy} = \frac{K_I}{\sqrt{2\pi R(\theta)}} cos\left(\frac{\theta}{2}\right) sin\left(\frac{\theta}{2}\right) sin\left(\frac{3\theta}{2}\right) \quad (1)$$
$$\sigma_{zz} = 0, \text{ for plane stress}$$
$$\sigma_{zz} = \nu(\sigma_{xx} + \sigma_{yy}), \text{ for plane strain}$$

where ν is Poisson ratio and $R(\theta)$ is radial distance from origin. K_I is called stress intensity factor (SIF). The principal stresses $\sigma_{1,2}$ can be obtained by transformations.

$$\sigma_{1,2} = \frac{\sigma_{xx} + \sigma_{yy}}{2} \pm \sqrt{\left(\frac{\sigma_{xx} - \sigma_{yy}}{2}\right)^2 + \left(\sigma_{xy}\right)^2} \quad (2)$$

Substituting equations (1) into (2), the principal stresses can be determined.

$$\sigma_1 = \frac{K_I}{\sqrt{2\pi R(\theta)}} cos\left(\frac{\theta}{2}\right)\left[1 + sin\left(\frac{\theta}{2}\right)\right]$$
$$\sigma_2 = \frac{K_I}{\sqrt{2\pi R(\theta)}} cos\left(\frac{\theta}{2}\right)\left[1 - sin\left(\frac{\theta}{2}\right)\right] \quad (3)$$
$$\sigma_3 = 0, \text{ for plane stress}$$
$$\sigma_3 = \frac{K_I}{\sqrt{2\pi R(\theta)}} cos\left(\frac{\theta}{2}\right), \text{ for plane strain}$$

$R(\theta)$, the boundary of PZ, will be obtained by substitution Equation (3) into a yield criterion and solved for *R(θ)* for plane stress or strain states separately. For calculation, an *m* file is written using Matlab© [15].

3.2 Yield Criteria

A stress state can be transformed to an equivalent stress value by means of yield criterion's equation. So a yield criterion is a convenient tool to compare it to the material's yield strength to determine whether plastic deformation is started or not. In this study, equivalent stress is determined by using isotropic yield criteria such as Von Mises [16], Tresca [17], and anisotropic yield criteria such as Hill48 [18] and Hu2003 [19]. General equation of the Von Mises yield function is given in Equation (4).

$$f(\sigma_{ij}) = \emptyset(\sigma_{1,2,3}) - (\bar{\sigma})^2 = 0$$
$$\emptyset(\sigma_{1,2,3}) = \frac{|\sigma_1 - \sigma_2|^2 + |\sigma_2 - \sigma_3|^2 + |\sigma_3 - \sigma_1|^2}{2} \quad (4)$$

where $\bar{\sigma}$ is the equivalent stress, $\emptyset(\sigma_{1,2,3})$ is its yield function and $\sigma_{1,2,3}$ are principal stresses. Similarly, the Tresca yield function is given in Equation (5).

$$f(\sigma_{ij}) = \emptyset(\sigma_{1,2,3}) = (\bar{\sigma}) \quad (5a)$$
$$\emptyset(\sigma_{1,2,3}) = max(|\sigma_1 - \sigma_2|, |\sigma_2 - \sigma_3|, |\sigma_3 - \sigma_1|) \quad (5b)$$

The quadratic Hill48 yield function is given in Equation (6a). Equation (6b) can be written when anisotropy axes are orthogonal. Its simultaneous solution with Equation (6b) gives Equation (6c).

$$2f(\sigma_{ij}) = F(\sigma_2 - \sigma_3)^2 + G(\sigma_3 - \sigma_1)^2 + H(\sigma_1 - \sigma_2)^2 = 1 \quad (6a)$$

$$(H + G).(\sigma_1)_y^2 = 1$$
$$(F + H).(\sigma_2)_y^2 = 1$$
$$(F + G).(\sigma_3)_y^2 = 1$$
$$F = \frac{(\sigma_0)^2}{2}\left[-\frac{1}{(\sigma_1)_y^2} + \frac{1}{(\sigma_2)_y^2} + \frac{1}{(\sigma_3)_y^2}\right]$$
$$G = \frac{(\sigma_0)^2}{2}\left[\frac{1}{(\sigma_1)_y^2} - \frac{1}{(\sigma_2)_y^2} + \frac{1}{(\sigma_3)_y^2}\right] \quad (6b)$$
$$H = \frac{(\sigma_0)^2}{2}\left[\frac{1}{(\sigma_1)_y^2} + \frac{1}{(\sigma_2)_y^2} - \frac{1}{(\sigma_3)_y^2}\right]$$
$$L = \frac{1}{2(\tau_{23})_y^2} = \frac{3(\tau_0)^2}{2(\tau_{23})_y^2}$$
$$M = \frac{1}{2(\tau_{31})_y^2} = \frac{3(\tau_0)^2}{2(\tau_{31})_y^2}$$
$$N = \frac{1}{2(\tau_{12})_y^2} = \frac{3(\tau_0)^2}{2(\tau_{12})_y^2} \text{ where } \tau_0 = \frac{\sigma_0}{\sqrt{3}}$$

$$F(\sigma_2 - \sigma_3)^2 + G(\sigma_3 - \sigma_1)^2 + H(\sigma_1 - \sigma_2)^2 = (\sigma_0)^2 = \bar{\sigma}^2 \quad (6c)$$

where $(\sigma_1)_y$, $(\sigma_2)_y$, and $(\sigma_3)_y$ are the normal yield stresses with respect to the principal anisotropy axes and $(\tau_{23})_y$, $(\tau_{31})_y$, and $(\tau_{12})_y$ are the yield stresses in shear with respect to the axes of anisotropy and τ_0, σ_0 are reference yield stress. It is assumed that the reference axes are on the principle anisotropy axes, which are orthogonal. As a special case, Hill48 criterion becomes Von Mises criterion when *F* = 1/2, *G* = 1/2, *H* = 1/2. This case will be used for comparison/verification of the Hill48 equations. Also the coefficients *G*, *H*, *F* are calculated by using anisotropy values as in Equation (7) [20].

$$F = \frac{r_0}{r_{90}(r_0+1)}, \quad G = \frac{1}{r_0+1}, \quad H = \frac{r_0}{r_0+1} \quad (7)$$

These coefficients are calculated as *F*=0.5263158, *G*=0.5263158, *H*=0.4736842 while $r_0 = 0.9$, $r_{45} = 1.1$, $r_{90} = 0.9$. The quadratic Hill48 yield function is reduced as in Equation (8) for plane stress condition as a special case. To make comparison, both equations are evaluated.

$$(\sigma_1)^2 + \frac{r_0(1+r_{90})}{r_{90}(1+r_0)}(\sigma_2)^2 - \frac{2r_0}{1+r_0}\sigma_1\sigma_2 = \bar{\sigma}^2 \quad (8)$$

Lastly, a generalized equation of Hu2003 yield criterion is given in Equation (9).

$$f(\sigma_{ij}) = \frac{1}{\sigma_0^4}\sigma_1^4 - \frac{4r_0}{(1+r_0)\sigma_0^4}\sigma_1^3\sigma_2 + (\frac{1}{\sigma_b^4} - \frac{1}{\sigma_0^4} - \frac{1}{\sigma_{90}^4} + \frac{4r_0}{(1+r_0)\sigma_0^4} + \frac{4r_{90}}{(1+r_{90})\sigma_{90}^4})\sigma_1^2\sigma_2^2 - \frac{4r_{90}}{(1+r_{90})\sigma_{90}^4}\sigma_1\sigma_2^3 + \frac{1}{\sigma_{90}^4}\sigma_2^4 = 1 \quad (9)$$

where $\sigma_0, \sigma_{45}, \sigma_{90}$ are yield stresses at the direction 0°, 45°, 90° with respect to rolling direction and σ_b is yield stress from equi-biaxial test. Equivalent stress formula can be obtained from this equation by solving it for σ_0 which it is also called equivalent stress.

3.3 Plastic Zone Equations

It was assumed that the boundary of this zone was just as a simple circle at the beginning of fracture mechanics. In Equation (10), the first approximation for PZ size for plane stress case is given. It defines just a constant circle whose left quadrant is located at the crack tip [21].

$$R(\theta)_{dg} = \frac{1}{2\cdot\pi}\left(\frac{K_1}{\sigma_y}\right)^2 \quad (10)$$

where $R(\theta)_{dg}$ stands for the plain stress state case, $R(\theta)_{dsd}$ shows the plain strain state case. Later, Irwin [22] assumed that the radius of PZ would be greater twice. It is seen in Equation (11). It estimates PZ for isotropic materials under mode-I loading.

$$R(\theta)_{dg} = \frac{1}{\pi}\left(\frac{K_1}{\sigma_y}\right)^2 \quad (11)$$

In Equation (12), Dugdale's formula [23] presented another circle with greater diameter than Irwin's circle.

$$R(\theta)_{dg} = \frac{\pi}{8}\left(\frac{K_1}{\sigma_y}\right)^2 \quad (12)$$

These formulas do not take care of θ-dependence of PZ size and just calculate $R(\theta)$ at θ=0. Actually, the PZ size depends on yield criterion; materials strain hardening and thickness. In any loading case, while the outmost surface of the bodies is subjected to plane stress state, it is getting become plain strain state towards inner surface. As a yield criterion gives the elasto-plastic boundary, a PZ boundary becomes a yield boundary when it is solved by using a yield criterion. PZ is obtained by substitution stress field into the yield criterion and then solved for radius $R(\theta)$. Because crack initiation starts at the outer surface first, plane stress equations are used in the scope of this study. When the yield criterion is Von Mises, PZ equations will become as in Equation (13).

$$R(\theta)_{dg} = -\frac{1}{2\pi}\left(\frac{K_1}{\bar{\sigma}}\right)^2\left(\frac{1+\cos\theta}{2}\right)\left(\frac{3\cos\theta}{2} - \frac{5}{2}\right) \quad (13a)$$

$$R(\theta)_{dsd} = -\frac{1}{2\pi}\left(\frac{K_1}{\bar{\sigma}}\right)^2\left(\frac{1+\cos\theta}{2}\right)\left(-4\nu^2 + 4\nu + \left(\frac{3\cdot\cos\theta}{2} - \frac{5}{2}\right)\right) \quad (13b)$$

It is seen that when θ=0 then Equation (13*a*) becomes Equation (10). Both equations are validated by comparing to Equation (14) derived for mode-I case using Von Mises criterion [24, 25]. Its graphics are given in subsequent sections.

$$R(\theta)_{dg} = \frac{1}{4\cdot\pi}\left(\frac{K_1}{\bar{\sigma}}\right)^2\left(1 + \cos\theta + \frac{3}{2}\sin^2\theta\right) \quad (14a)$$

$$R(\theta)_{dsd} = \frac{1}{4\cdot\pi}\left(\frac{K_1}{\bar{\sigma}}\right)^2\left((1+\cos\theta)(1-2\nu^2) + \frac{3}{2}\sin^2\theta\right) \quad (14b)$$

Similarly, results from Tresca criterion [25] are obtained as in Equation (15)

$$R(\theta)_{dg} = \frac{1}{2\pi}\left(\frac{K_1}{\bar{\sigma}}\right)^2\left(\frac{\cos\theta}{2} + \frac{1}{2}\right)\left(\sin\frac{\theta}{2} + 1\right)^2 \quad (15a)$$

$$R(\theta)_{dsd} = \frac{1}{8\pi}\left(\frac{K_1}{\bar{\sigma}}\right)^2\left(2*\cos\frac{\theta}{2} + \sin\theta - 4\nu\cos\frac{\theta}{2}\right)^2 \quad (15b)$$

Both equations are validated by comparing to Equation (16) derived for mode-I case using Tresca criterion [25].

$$R(\theta)_{dg} = \frac{1}{2\cdot\pi}\left(\frac{K_1}{\bar{\sigma}}\right)^2\left(\cos\frac{\theta}{2} + abs(\cos\frac{\theta}{2}\sin\frac{\theta}{2})\right)^2 \quad (16a)$$

$$R(\theta)_{dsd} = \frac{1}{2\cdot\pi}\left(\frac{K_1}{\bar{\sigma}}\right)^2\left((1-2\nu)\cos\frac{\theta}{2} + abs(\cos\frac{\theta}{2}\sin\frac{\theta}{2})\right)^2 \quad (16b)$$

Similarly, results from Hill48 are seen in Equation (17).

$$R(\theta)_{dg} = \frac{1}{2\cdot\pi}\left(\frac{K_1}{\bar{\sigma}}\right)^2\left(\frac{1+\cos\theta}{2}\right)\left(F + G + (F + G + 4H)\sin(\frac{\theta}{2})^2 + (2G - 2F)\sin(\frac{\theta}{2})\right) \quad (17a)$$

$$R(\theta)_{dsd} = \frac{1}{2\cdot\pi}\left(\frac{K_1}{\bar{\sigma}}\right)^2\left(\frac{1+\cos\theta}{2}\right)\left(F + G - 4F\nu - 4G\nu + 4F\nu^2 + 4G\nu^2 + (F + G + 4H)\sin(\frac{\theta}{2})^2 + (-2F + 2G + 4F\nu - 4G\nu)\sin\left(\frac{\theta}{2}\right)\right) \quad (17b)$$

Result from quadratic Hill48 is seen in Equation (18). It is just for the plain stress state case.

$$R(\theta)_{dg} = \frac{1}{2\cdot\pi}\left(\frac{K_1}{\bar{\sigma}}\right)^2\left(\frac{1+\cos\theta}{2}\right)\left(\left(\sin\left(\frac{\theta}{2}\right) + 1\right)^2\right) - H(\cos(\theta) + 1) + \left(F\left(\sin\left(\frac{\theta}{2}\right) - 1\right)^2 * (r_{90} + 1)\right) \quad (18)$$

Result for plastic zone size calculations by using Hu2003 criterion is as follow.

$$R(\theta)_{dg} = \frac{1}{2\cdot\pi}\left(\frac{K_1}{\bar{\sigma}\,\sigma_{90}\,\sigma_b}\right)^2\left(\frac{1+\cos\theta}{2}\right)\Big|\sigma_{90}{}^4\bar{\sigma}^4 + \left(4\sigma_b^4\sigma_{90}{}^4 - 4\sigma_b^4\bar{\sigma}^4 - 8H\sigma_{90}{}^4\sigma_b^4 + 8HU\bar{\sigma}^4\sigma_b^4\right)sin\left(\frac{\theta}{2}\right) + \left(8\sigma_{90}{}^4\sigma_b^4 - 2\sigma_{90}^4 + 8\bar{\sigma}^4\sigma_b^4 - 8H\sigma_{90}{}^4\sigma_b^4 - 8HU\bar{\sigma}^4\sigma_b^4\right)\left(sin\left(\frac{\theta}{2}\right)\right)^2 + \left(4\sigma_{90}{}^4\sigma_b^4 - 4\bar{\sigma}^4\sigma_b^4 + 8H\sigma_{90}{}^4 6_b^4 - 8HU\bar{\sigma}^4\sigma_b^4\right)\left(sin\left(\frac{\theta}{2}\right)\right)^3 + \left(\sigma_{90}{}^4\bar{\sigma}^4 + 8H\sigma_{90}{}^4\sigma_b^4 + 8HU\bar{\sigma}^4\sigma_b^4\right)\left(sin\left(\frac{\theta}{2}\right)\right)^4\Big|^{1/2} \quad (19)$$

where $HU=r_{90}/(r_{90}+1)$.

3.4 Finite Element Analysis of Elasto-Plastic Pipe Containing A Semi Elliptical Surface Crack

Analysis is performed on the pipe's three-dimensional finite element model by using Ansys© [26], as shown in Figure 3. Its fracture module is used for crack insertion. It first calculates the energy at the crack tip (this energy is called the *J*-integral). Then the SIF (K_I), is calculated using the *J*-integral [13].

The dimensions of the model is taken the same with the pipe. No symmetry conditions are applied. A semi-elliptical crack is inserted on the surface of the pipe. The crack is parallel to pipe's cross-section. Tetragonal elements are used in order to obtain good match between crack's and pipe body's elements. While one end of the pipe is fixed, a uniform 560 MPa remote tensile stress is applied to the surface normal of the other end. It causes to yield the material in PZ. So mode-I condition is guaranteed. Analysis is performed using BISO rule to ensure elasto-plastic behavior. Analysis has both material nonlinearity and large deformation. So a nonlinear structural analysis is performed in 20 load steps. Geometry is updated in each iteration. No contact is used.

The parameters necessary to define the semi-elliptical crack are shown on Figure 4. The crack tip curve is divided into 100 front elements. FEA uses domain integral over counters in the crack tip, so 6 counters which surround the crack curve are set. The largest counter radius is taken as 0.01mm.

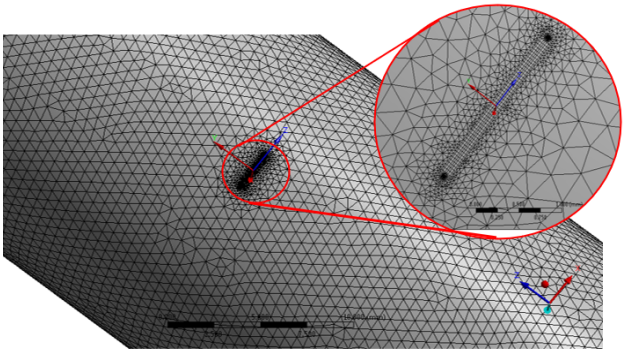

Figure 3. The location of the crack on the meshed model.

Element grow rate is 1.2 through crack tip ligament. The model includes 145987 elements in total after finite element meshing.

It is reported that when compared with the rigorous solution which is a type of analytical solution, the error on SIF values is less than 1% in the interval 0.0001mm<*r*<0.01mm where *r* is radial distance from the crack tip [27]. Thus, it is clear that the stress intensity factor fund in this range can be trustable. So the SIF obtained from FEA can meet the requirements of engineering applications. Taking that the length of the element in the crack tip is 0.002 mm, we ensure that it stays in the range and is enough to be able to catch SIF with error less than 1%.

4. Results and Discussion

4.1 SIF Solutions

The stress intensity factors (SIF, K_I) obtained from FEA are seen in Figure 5. Results are based on contours which surround the crack curve. The innermost is counter 1. The most critical SIF value may be seen either at the surface (*B*) or at the deepest point (*A*) generally. The figure includes 6 curves for 6 counters surrounding the crack tip.

The higher SIF means the more resistance to crack initiation. So, the minimum $K_I = 0.73582\ MPa\sqrt{mm}$ will be considered.

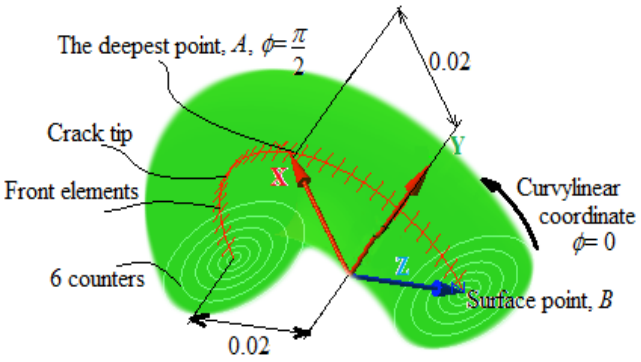

Figure 4. Parameters of the semi-elliptical surface crack

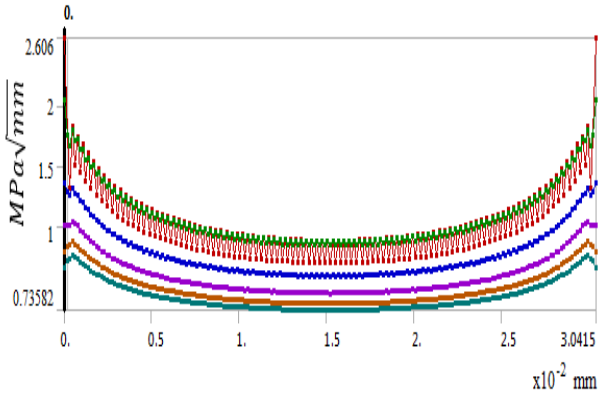

Figure 5. SIF results in the crack front

4.2 Plastic Zone Sizes

PZ equations are drawn using those numerical values. SIF is taken as $K_1 = 0.73582\ MPa\sqrt{mm}$. A polar coordinate axis is located at the crack tip and θ is taken between 0-360°. The yield strength is substituted for $\bar{\sigma}$. For verification, the Von Mises based PZ equations (13) are compared to Equation (14) [24, 25]. The Tresca based PZ equations (15) are compared to Equation (16) [24, 25] as seen in Figure 6. It is seen that curves have the same sizes [8, 28]. A self-comparison between the quadratic Hill48 and specific Hill48 for plane stress based PZ equations is done on Figure 7. It is verified that both of Equation (16, 18) draw the same zone size. Figure 7 also includes PZs from Irwin, Dugdale and first approximation equations for comparison.

As seen in Figure 8, the darker blue line is obtained when *F*=1/2, *G*=1/2, *H* = 1/2 where Hill48 equation turns to Von Mises equation. So, these equations are completely consistent with the ones shown by [29, 30].

4.3 Anisotropy Dependencies

For Hill48 and Hu2003 criteria, *F, G, H, N, M,* and *HU* coefficients depend on anisotropy coefficients r_0, r_{45}, r_{90}. By changing the anisotropy coefficients from $r_{45} = 1.1$, $r_{90} = 0.9$ to zero gradually, PZs are drawn. Figure 8, 9 show anisotropy dependencies of PZs based on Hill48 and Hu2003 criteria. Results are verified using the fact that Hill48 criterion becomes Von Mises criterion when *F* = 1/2, *G* = 1/2, *H* = 1/2. In literature, any study including Hu2003 is not seen. So the obtained results from Hu2003 equations are just given. At first sight, it is seen that the Hu's PZ size is much smaller than that of Tresca but bigger than that of Hill48.

It is noted that when anisotropy increases, the zone shape transits kidney to butterfly-like shape. While, PZ at the cracked-plane direction is getting shorten, its size is increasing at ± 30°-60°. It will affect the crack initiation angle because the larger PZ produces the higher SIF due to the more energy requirement for plastic deformation. *R*-criterion [31] is one of the criteria used to predict crack propagation path based on PZ's size.

4.4 FEA Results

The nonlinear structural analysis takes 7 hours 56 minutes on the computer with 4 GB RAM and 2.4 GHz CPU. Equivalent total strain and stress developed on the crack tip are seen in Figure 10 and 11. As expected, stress becomes constant after yield starts because perfect plastic material model has no hardening behavior. Diddering on the straight section of the curve is due to residuals on each increment in the load steps. Stress counters and strain iso-lines show that PZ takes butterfly-like shape at the crack tip through the crack curve.

4.5 Blunting of the Crack Tip

Figures 12 shows blunting of the crack tip. It is drawn by exaggerating 100 times. Bluntness cause to shape change at the crack tip. After deformation, no skewness on the crack tip elements are seen. This comparison implies no complication during blunting.

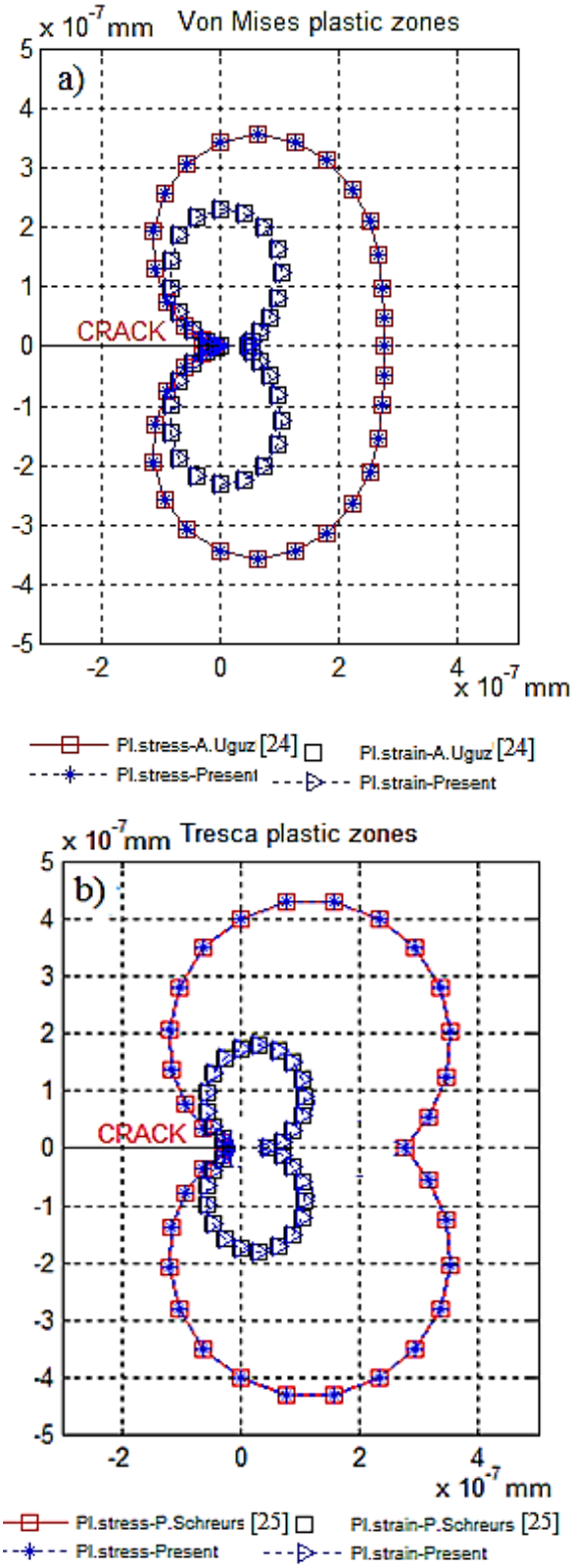

Figure 6. Comparisons of plastic zone sizes based on (*a*) Von Mises and (*b*) Tresca

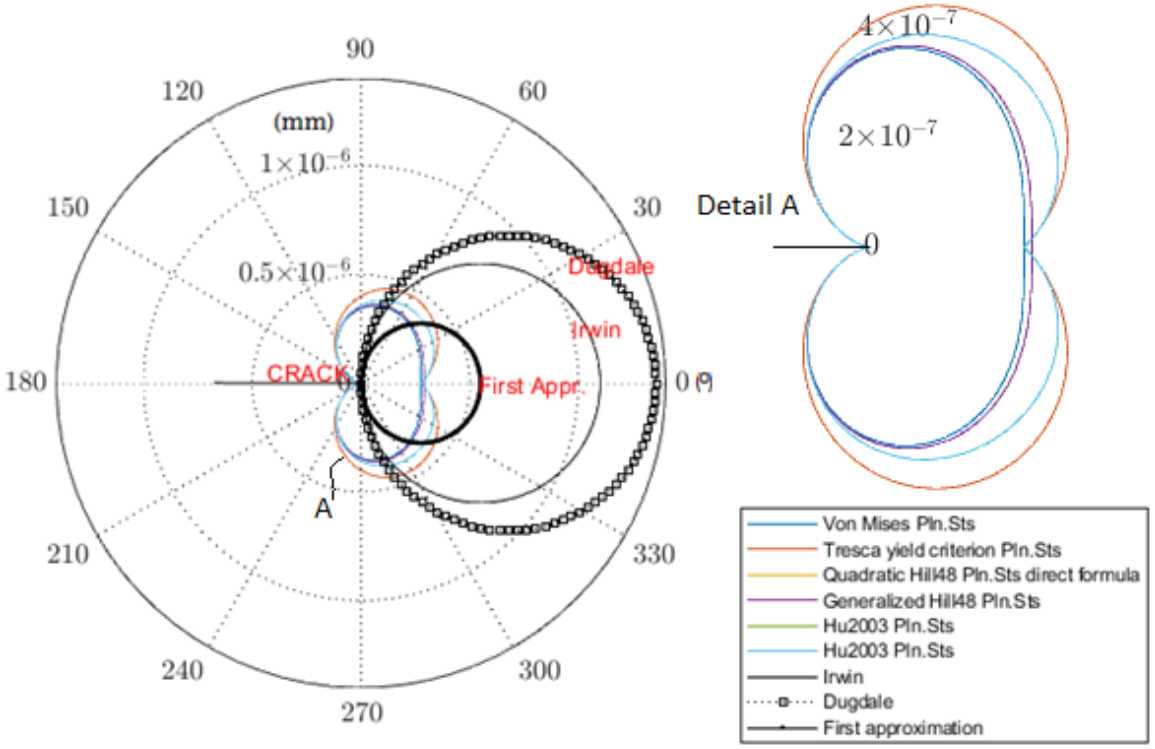

Figure 7. Plastic zones sizes based on various criteria

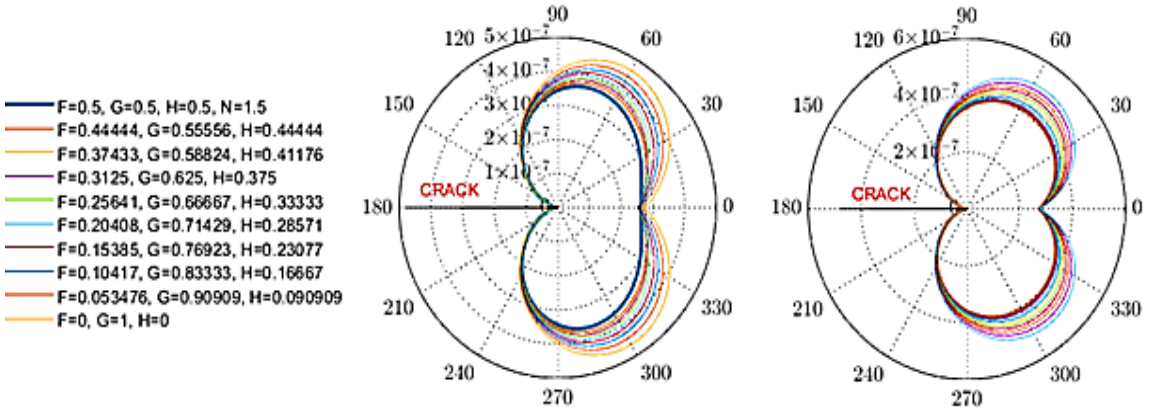

Figure 8. While r_0 *and* r_{90} change, PZ based on (*a*) Hill48 and (*b*) Hu2003

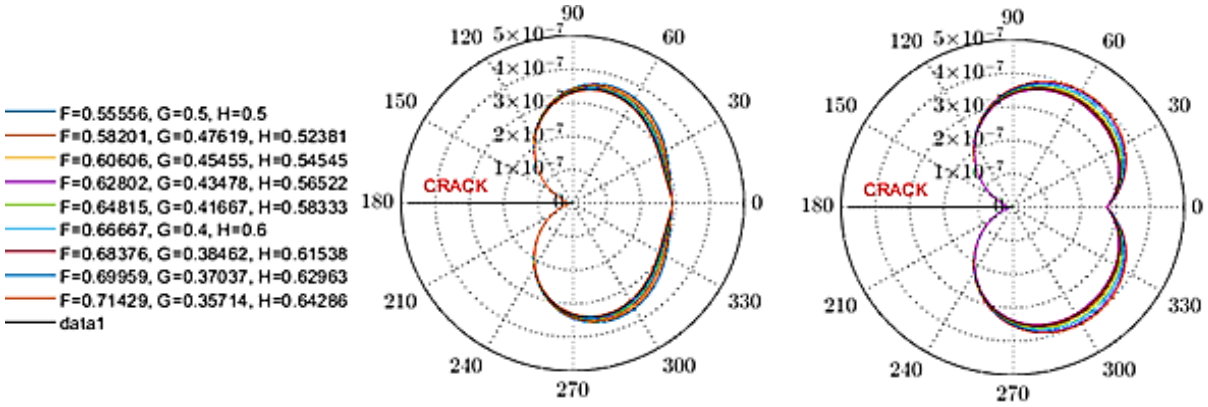

Figure 9. While r_0 *and* r_{45} change, PZ based on (*a*) Hill48 and (*b*) Hu2003

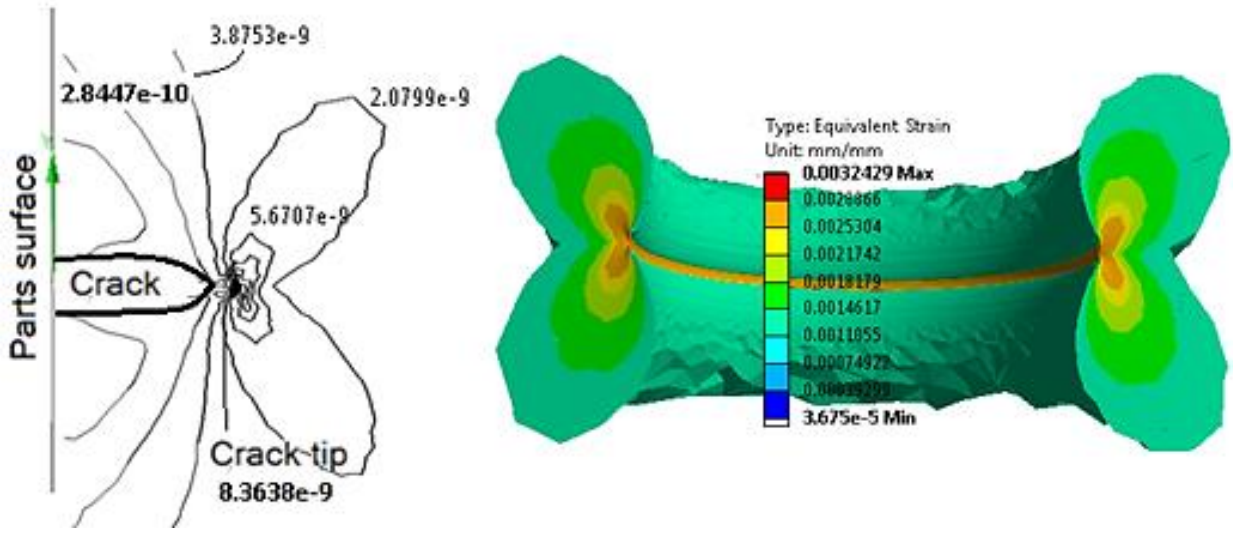

Figure 10. Equivalent strain iso-lines and 3D model from FEA (Unit: mm/mm)

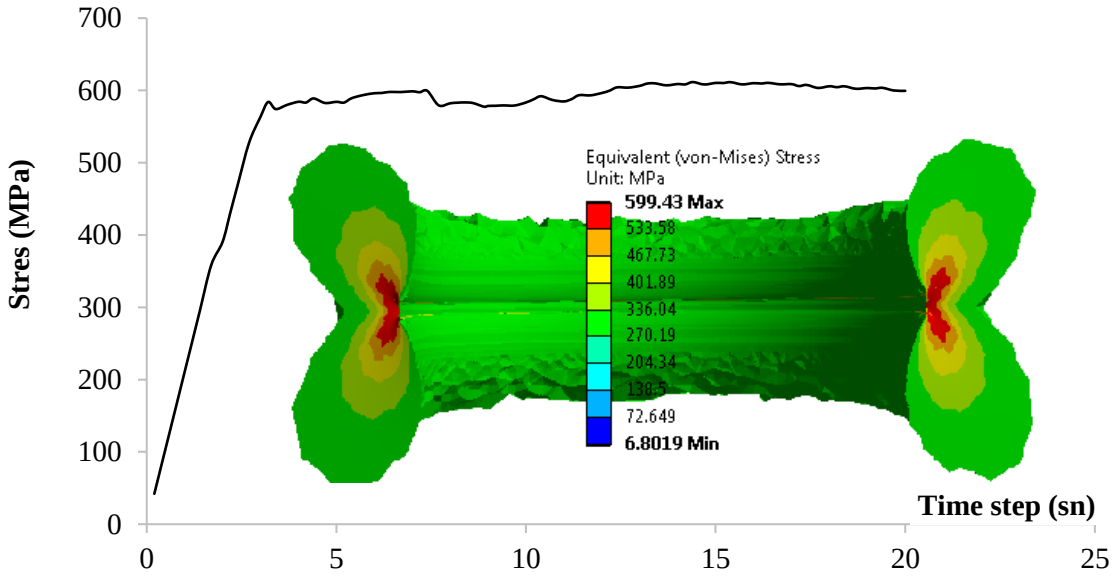

Figure 11. Equivalent stress distribution along the crack tip curve

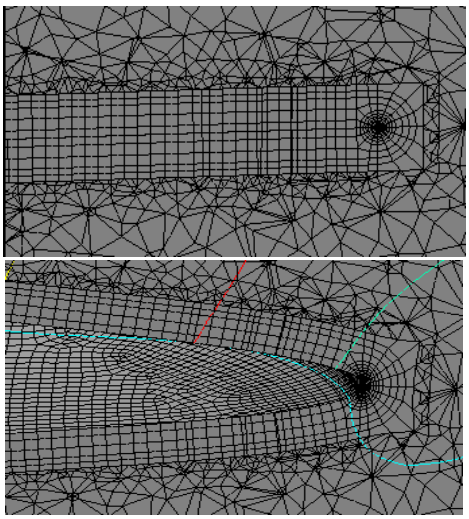

Figure 12. Crack tip profile *a*) before loading *b*) blunting after loading

5. Conclusions

PZs are necessary for calculation of crack propagation path. PZ's shape and size are analyzed for different anisotropy conditions. SIFs are obtained by performing a finite element simulation under isotropic and large-scale plasticity conditions. Also stress, strain distribution and blunting of the crack tip is given. So the following inferences are concluded.

- PZ sizes are obtained for the pipe made from 41Cr4 sheet metal by using four yield criteria: the Von Mises, Tresca, Hill48, and Hu2003.
- Results obtained from the Von Mises and Tresca verify that the derived equations provide the same shapes with literature. The area of PZ based on Tresca is larger than that of the Von Mises. The larger PZ leads to the higher SIF.

- Hill48-based PZ equation is verified using the fact that the equation must turn to Von Mises equation when F=1/2,G=1/2, H = 1/2.
- With respect to rolling direction, especially transverse anisotropy has higher effect on the PZ in the equation based on Hill48 and Hu2003. While PZ size increases for increasing anisotropy in transverse direction, PZ size decreases for increasing anisotropy at 45°. Increasing anisotropy affects the PZ's size.
- For increasing transverse anisotropy, Hill48-based PZ's shape transits from kidney to butterfly shape. Similarly, it transits from kidney to hearth shape for increasing anisotropy at 45°, it is a characteristic shape generally seen for increasing shear stresses or inclined angle in some cases.
- It is seen that stress becomes constant when material starts to yield due to no hardening in perfect plastic nature of selected hardening model.

Within the scope of this study, PZs are obtained. Crack propagation analyses will be performed as a future work.

Declaration

The author declared no potential conflicts of interest with respect to the research, authorship, and/or publication of this article. The author(s) also declared that this article is original and prepared in accordance with international publication and research ethics. Neither ethical committee permission nor special permission is required.

References

1. Alizadeh Kaklar, J. and H. Saeidi Googarchin, *Approximate stress intensity factors for a semi-circular crack in an arbitrary structure under arbitrary mode I loading.* Theoretical and Applied Fracture Mechanics, 2018. **94**: p. 71-83.
2. Burcham, M.N., et al., *Characterization and Failure Analysis of an Automotive Ball Joint.* Journal of Failure Analysis and Prevention, 2017. **17**(2/2017): p. 13.
3. Uguz, A. and S.H. Oka, *Modeling the effects of mechanical loads - Finite element modeling of ball joints under dynamic loading.* Materialpruefung/Materials Testing, 2004. **46**: p. 506-512.
4. Verim Ö. and M. Yumurtacı, *Application of reverse engineering approach on a damaged mechanical part.* International Advanced Researches and Engineering Journal, 2020. **4**(1): p. 21-28.
5. Do, T.D., et al., *Determination of Plastic Zone Sizes at the Crack Tip*. Materials Characterization: Modern Methods and Applications, 2016: p. 175-197.
6. Yi, Z.H. and S. Sun, *Thickness Effect on Fracture Toughness and Plastic Zone Size.* Proceedings of the 2010 International Conference on Mechanical, Industrial, and Manufacturing Technologies (Mimt 2010), 2010: p. 1-5.
7. Armentani, E., et al., *Plastic zone size as EPFM parameter.* Advances in Fracture and Damage Mechanics, 2003. **251-2**: p. 173-178.
8. Gao, X., et al., *Analytic solutions to crack tip plastic zone under various loading conditions.* European Journal of Mechanics a-Solids, 2010. **29**(4): p. 738-745.
9. Adetifa, O.A., *Estimating Plastic Zone Sizes for Edge Cracks.* International Journal of Fracture, 1984. **24**(4): p. R115-R120.
10. MakeItFrom. *Hardened (+H) 1.7035 Steel*. 2020 February 25.2019]; Available from: https://www.makeitfrom.com/material-properties/Hardened-H-1.7035-Steel.
11. Creese, R.C., *Introduction to Manufacturing Processes and Materials*. 1999: CRC Press, Taylor and Francis Group.
12. Tada, H., P.C. Paris, and G.R. Irwin, *The Stress Analysis of Cracks Handbook*. 1973, Hellertown, Pennsylvania: Del. Research Corporation.
13. Kacar, İ., *Fracture mechanics: weight function method*, in *Academic Studies in Engineering Sciences-2019/2*, T.Y. Ali Kılıçer, Editor. 2019, Ivpe press: Cetinje-Montenegro, Cetinje, Montenegro. p. 149-173.
14. Kacar, İ., *An example application for calculating the stress intensity factor by using the weight function method*, in *Academic Studies in Engineering Sciences-2019/2*, T.Y. Ali Kılıçer, Editor. 2019, Ivpe press: Cetinje-Montenegro, Cetinje, Montenegro. p. 174-188.
15. MathWorks Inc, *MATLAB : the language of technical computing : computation, visualization, programming : installation guide for UNIX version 5*. 1996: Natwick : Math Works Inc., 1996.
16. Mises, R.V., *Mechanics of solid bodies in the plastically-deformable state.* Mathematisch-physikalische Klasse, 1913. **1**: p. 582-592.
17. Nadai, A., *Theory of flow and fracture of solids*. 2nd ed. ed. Engineering societies monographs. 1950: New York, NY : McGraw-Hill.
18. Hill, R., *A theory of the yielding and plastic flow of anisotropic metals.* Mathematical, Physical and Engineering Sciences, 1948. **193**(1033): p. 281-297.
19. Kılıç S., Toros S., Kacar İ and Fahrettin Ö., *Sonlu Elemanlar Analizlerinde Sac Metal Şekillendirme Parametrelerinin İncelenmesi*, in *Geleceğin Dünyasında Bilimsel ve Mesleki Çalışmalar-Mühendislik ve Teknoloji*, Ö.T. M. Lüy, E. Çam, N. Barışçı, M. D. Demirbaş & M. Güçyetmez, Editor. 2018, Ekin Basım Yayın Dağıtım: Bursa.
20. Colby, R.B., *Equivalent Plastic Strain for the Hill's Yield Criterion under General Three-Dimensional Loading*, in *Department of Mechanical Engineering at the Massachusetts Institute of Technology*. 2013, Massachusetts Institute of Technology: Massachusetts Institute of Technology. p. 45.
21. Sun, C.T. and Z.H. Jin, *Chapter 6 - Crack Tip Plasticity*, in *Fracture Mechanics*, C.T. Sun and Z.H. Jin, Editors. 2012, Academic Press: Boston. p. 123-169.
22. Irwin, G.R., *Plastic Zone Near a Crack Tip and Fracture Toughness*, in *Sagamore Ordnance Material Conference*. 1960. p. IV63–1V78.
23. Dugdale, D.S., *Yielding of steel sheets containing slits.* Journal of the Mechanics and Physics of Solids, 1960. **8**(2): p. 100-104.
24. Uğuz, A., *Kırılma Mekaniğine Giriş*. 1.Baskı ed. 1996, Bursa: Vipaş Yayınları.
25. Schreurs, P. *Fracture Mechanics (4A780)*. 2020 [cited 2020 January, 2020]; Available from:

http://www.mate.tue.nl/~piet/edu/frm/htm/frmnum1112.html.

26. DeSalvo, G.J. and J.A. Swanson, *ANSYS engineering analysis system user's manual*. 1985, Houston, Pa: Swanson Analysis Systems.
27. Ji, X., F. Zhu, and P.F. He, *Determination of stress intensity factor with direct stress approach using finite element analysis.* Acta Mechanica Sinica, 2017. **33**(5): p. 879-885.
28. Ivey, J., *Analytic Solutions for the Crack-Tip Plastic Zone under Mixed Mode Loading Conditions*, in *Mechanical Engineering*. 2017, University of New Mexico: Albuquerque, New Mexico.
29. Khan, S.M.A. and M.K. Khraisheh, *The anisotropic R-criterion for crack initiation.* Engineering Fracture Mechanics, 2008. **75**(14): p. 4257-4278.
30. Cao, J., et al., *Study of anisotropic crack growth behavior for aluminum alloy 7050-T7451*. Engineering Fracture Mechanics, 2018. **196**: p. 98-112.
31. Khan, S.M.A. and M.K. Khraisheh, *A new criterion for mixed mode fracture initiation based on the crack tip plastic core region.* International Journal of Plasticity, 2004. **20**(1): p. 55-84.